MOVING SINGULARITIES OF THE FORCED FISHER–KPP EQUATION: AN ASYMPTOTIC APPROACH*

MARKUS KACZVINSZKI† AND STEFAN BRAUN†

Abstract. The creation of hairpin or lambda vortices, typical for the early stages of the laminar-turbulent transition process in various boundary layer flows, in some sense may be associated with blow-up solutions of the Fisher–KPP equation. In contrary to the usual applications of this nonlinear evolution equation of reaction-diffusion type, the solution quantity in the present context neither needs to stay bounded nor positive. We focus on the solution behavior beyond a finite-time point blow-up event, which constitutes two moving singularities (representing the cores of the vortex legs) propagating in opposite directions, and their initial motion is determined with the method of matched asymptotic expansions. After resolving subtleties concerning the transition between logarithmic and algebraic expansion terms in the regarding asymptotic layers, we find that the internal singularity structure resembles a combination of second and first order poles in form of a singular traveling wave with a time-dependent speed imprinted through the characteristics of the preceding blow-up event.

Key words. Singularity tracking, nonlinear dynamics, asymptotic analysis, Chebyshev spectral collocation, laminar-turbulent transition

MSC codes. 35C20, 76M45, 76D10, 35K57, 76F06, 65L10

1. Introduction and problem formulation. The present study deals with real-valued, singular solutions of the forced Fisher–Kolmogorov–Petrowsky–Piscounov (Fisher–KPP) equation [10, 18],

$$\frac{\partial u}{\partial t} - \frac{\partial^2 u}{\partial z^2} = u - u^2 + g\,, \tag{1.1}$$

that occur immediately *beyond* a finite-time blow-up event $|u| \to \infty$ as $t \to t_s$, $z \to z_s$, where (z_s, t_s) denotes the blow-up point. It is important to note that in the present case $u(z,t) \in \mathbb{R}$ is assumed to cover the full range, and $z \in \mathbb{R}$ is the spatial coordinate and $t \in \mathbb{R}_0^+$ the time. The only function of the forcing term $g(z,t) \sim O(1)$ is to provoke the formation of a localized finite-time singularity when starting e.g. from the initial condition $u(z,0) = 1$, i.e. the stable/attracting stationary state $u_s = 1$ ($u_s = 0$ is unstable/repelling). Once a point blow-up event is triggered, independent of how, the linear term u and the forcing g play a subordinate role in the immediate vicinity of the blow-up point (the focus of our study), where a subtle balance between the time-derivative, the diffusion and the quadratic nonlinearity terms of (1.1) holds, [16, 13]. For a physical motivation of equation (1.1) in the present, rather unusual, setting the interested reader is referred to appendix B and references cited therein.

As is well-known, nonlinear reaction-diffusion equations of the (unforced) Fisher–KPP type commonly occur in two contexts. The first area is population dynamics and genetics, where the solution pictures the evolution of some concentration, i.e. a strictly bounded quantity, $u \in [0,1]$. In that case travelling wave solutions $u(z,t) = v(\xi)$, $\xi = z - ct - \xi_0$ are of particular significance, e.g. [19]. Here ξ, c denote the wave coordinate, wave speed and the arbitrary constant ξ_0 accounts for the translation invariance of the wave profile. Due to the domain restrictions allowed solutions join

*Funding: This work was supported by the Austrian Science Fund FWF, Grant No. P 31873-N32.

†Institute of Fluid Mechanics and Heat Transfer, TU Wien, Getreidemarkt 9, 1060 Vienna, Austria. (markus.kaczvinszki@tuwien.ac.at, stefan.braun@tuwien.ac.at).

the stationary states $u_s = 0, 1$ (heteroclinic orbit in Poincaré's phase portrait) and have a wave speed of $|c| \geq 2$. The second typical application concerns the subject of semilinear heat equations, here the restriction $u \in (0, \infty)$ holds for the dependent variable (temperature), which requires a sign change $u \to -u$ (of the nonlinearity at the rhs) in (1.1), see e.g. the recent study [9] and references therein.

For some overview of the important aspects of finite-time blow-up we suggest the survey [13]. In particular relevant is the work by Fujita [11], where it is shown that the semilinear heat equation $u_t - u_{zz} = u^2$ always blows up for arbitrary small positive initial data. In contrast, blow-up criteria for generalized Fisher-KPP equations are formulated in [14] based on stationary solutions.

As in the present case, blow-up is denoted incomplete, if there exists an extended solution $u(z, t > t_s)$ which remains finite at most locations $z \in \mathbb{R}$. A characterization of complete or incomplete blow-up scenarios is given in [12], especially therein the semilinear heat equation with u^2-nonlinearity (mentioned above) is claimed to undergo complete blow-up. This appears incorrect in our present setting, since we neither have the restriction $u \geq 0$ nor is our solution continuous in time at (z_s, t_s), figure 1.

Possibly due to these reasons, there exist almost no relevant studies which deal with the solution behavior beyond blow-up. Only recently, Fasondini et al. [9] tried to numerically calculate post blow-up solutions of a semilinear heat equation with periodic boundary conditions, claiming that beyond t_s the solution is inherently complex-valued. We believe our results are more tangible and physically feasible, because the sought solution is solely real-valued. If, however, one considers an analytic continuation into the complex plane, complex-valued singularities indeed exist before the blow-up time t_s. They propagate from both sides of the imaginary axis towards the real axis where they eventually meet at t_s. There, due to the time-reflection relation between solutions immediately before and beyond blow-up (a special case of a scale-invariance property)

$$u(z - z_s, t - t_s) \sim -u(\pm i(z - z_s), t_s - t)\,, \quad \text{as} \quad t - t_s \to 0^{\pm},\ z - z_s \to 0^{\pm}, \tag{1.2}$$

a continuation to later times is possible where now a pair of real-valued singularities move away from the symmetry axis in opposite directions, [3]. The tracking of complex singularities before blow-up by means of sophisticated numerical techniques has been carried out by Weideman, [25]. Therein the application example of a semilinear heat equation is of particular interest in our context.

The aim of the present paper is to analytically compute the initial motion of the real-valued singularity pair beyond blow-up governed by (1.1) through the method of matched asymptotic expansions. It can be viewed as a continuation of the first attempts towards a solution by [3]. Apart from the remarkable physical interpretation of the generation of moving singularities beyond blow-up as the formation of vortex structures (kernels) close to the wall as depicted in figure 6, the study independently represents an interesting and challenging mathematical task. The paper is organized as follows. In section 2 we revisit the well-known asymptotic structure of blow-up solutions to (1.1) alongside with some basic considerations for studying asymptotic sublayers with the objective to obtain uniformly valid expansions. The technically complicated first sublayer, valid in the immediate proximity of the initial singularity, and the description of the required numerical computations regarding the second sublayer, are discussed in sections 3 and 4, respectively. The final results as well as an outlook are given in section 5, and the conclusions are drawn in section 6. Calculation details of our asymptotic approach as well as references to the physical background of the present study can be found in appendices A and B, respectively.

2. Blow-up solutions of the Fisher–KPP equation.

2.1. Finite time blow-up and pair generation. Let say the solution of the Fisher equation (1.1) blows up at some arbitrary position z_s and time t_s, then its asymptotically correct representation near the blow-up point (z_s, t_s) can be written down as a pseudo-similarity law [16, 8, 15, 3, 4],

$$u(z,t) \sim \frac{1}{t-t_s} f(\hat{z},\tau) + O\left((t-t_s)^0\right), \qquad t - t_s \to 0^{\pm}. \tag{2.1}$$

This local solution consists out of a temporal pole of first order and a pseudo blow-up profile f, which depends on the blow-up variable $\hat{z}$ and an exponentially short time scale τ, defined as

$$\hat{z} = \frac{z - z_s}{\sqrt{\tau |t - t_s|}}, \qquad \tau = -\ln|t - t_s| \to \infty. \tag{2.2}$$

While the blow-up variable $\hat{z}$ pictures the current spatial scaling, i.e. the relevant spatial distance $z - z_s$ in dependence of time t, the logarithmic time scale τ is the relevant temporal quantity for all of the upcoming asymptotic expansions.

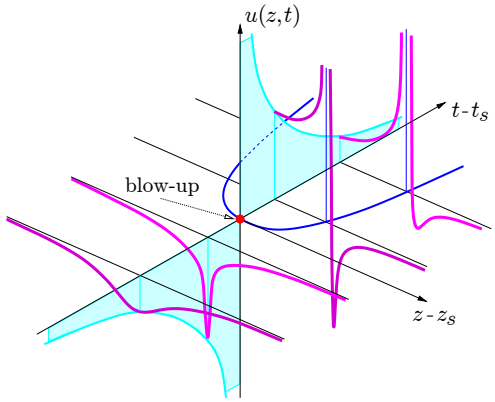

FIG. 1. *Schematic of the real-valued, asymptotic solution* (2.1), (2.4), *(magenta) of the Fisher equation (1.1) in the vicinity of a point blow-up event, [4]. Beyond blow-up, the (even) solution is depicted for $z > z_s$ only; the trajectories of the singularity pair are marked in blue.*

We insert ansatz (2.1) into the Fisher equation (1.1) and obtain the partial differential equation for f, omitting terms of $O(e^{-\tau})$ — i.e. u and g in (1.1),

$$\frac{\hat{z}}{2}\frac{\partial f}{\partial \hat{z}} - f^2 + f = \frac{1}{\tau}\left[\frac{\hat{z}}{2}\frac{\partial f}{\partial \hat{z}} \mp \frac{\partial^2 f}{\partial \hat{z}^2}\right] - \frac{\partial f}{\partial \tau}, \tag{2.3}$$

which can be asymptotically solved for $\tau \to \infty$ in agreement with $t - t_s \to 0^{\pm}$ of (2.1). The resulting expansion for f has the following form, [3]

$$f \sim \frac{8}{8 \mp \hat{z}^2} \pm \frac{10\hat{z}^2}{(8 \mp \hat{z}^2)^2}\frac{\ln(\tau)}{\tau} + \frac{16 \mp C_1 \hat{z}^2 \pm 8\hat{z}^2 \ln\left|8 \mp \hat{z}^2\right|}{(8 \mp \hat{z}^2)^2}\frac{1}{\tau} + O\left(\frac{\ln^2 \tau}{\tau^2}\right). \tag{2.4}$$

The lower sign corresponds to the solution shortly before the blow-up occurs at t_s and the upper sign to the extended solution shortly beyond t_s. Moreover, beginning

with the second temporal order $1/\tau$, some integration constants C_i appear. They correspond to the systems local degrees of freedom and may be fixed during a possible embedding into a global solution of u.

For a better understanding of this complicated structure, we have visualised the asymptotic solution of u in figure 1. Before blow-up the solution essentially consists of a minimum of increasing magnitude which reaches infinity at the blow-up time t_s. Then, a sudden sign change occurs and two singularities get created, which immediately propagate away from their creation point with decreasing speed. The dark blue line corresponds to the initial trajectory of this singularity pair, its spatio-temporal evolution will be discussed in the following and examined in detail in the upcoming sections.

2.2. Collapse and singular trajectory. We study the expansion (2.4) beyond t_s and see that it has a fixed spatial singularity location at $\hat{z} = \pm\sqrt{8}$. The expansion is not uniformly valid, it breaks down near this singularity position, since the spatial pole order increases alongside with the temporal expansion order. That means, there exists a spatial scaling around $\hat{z} = \pm\sqrt{8}$, where some or actually all expansion orders reach the same magnitude, such that the initial expansion ceases to be valid.

Because of the $\ln(\tau)$-contributions, the generation of the correct breakdown scaling has been an open problem for some time, cf. [3]. We solved it via equating different expansion orders to each other, here done for the first two orders,

$$\frac{8}{8-\hat{z}^2} \overset{!}{\sim} \frac{10\hat{z}^2}{\left(8-\hat{z}^2\right)^2}\frac{\ln(\tau)}{\tau} \overset{!}{\sim} \frac{8\hat{z}^2 \ln\left|8-\hat{z}^2\right|}{\left(8-\hat{z}^2\right)^2}\frac{1}{\tau}\,. \tag{2.5}$$

This comparison of magnitudes, e.g. between the first and second term, immediately yields the first inner variable (for the right and left running singularity respectively),

$$\gamma = \left(\hat{z} \mp \sqrt{8}\right)\frac{\tau}{\ln(\tau)} \sim O(1)\,. \tag{2.6}$$

In order to find out what happens inside the breakdown area of expansion (2.4), we zoom in treating γ as the next relevant spatial quantity of $O(1)$. We perform the corresponding change of variables in (2.3) and obtain a new differential equation and a new expansion, which holds valid information in the vicinity of the initial singularity position $\hat{z} = \pm\sqrt{8}$. In the next section we study this so-called first asymptotic sublayer in detail, but for now we want to give some overview of our general approach.

In particular, the expansion of the first asymptotic sublayer has again a singularity position and again undergoes breakdown near this singularity. That means we can once more introduce a new spatial scaling and actually repeat this zooming process infinitely long, and thereby we obtain the step-wise correction of the initial motion of the singularity pair,

$$\hat{z}_p = \frac{z_p - z_s}{\sqrt{\tau(t-t_s)}} \sim \pm\sqrt{8}\left[1 - \frac{1}{8}\frac{\ln(\tau)}{\tau} + \frac{\zeta_s}{4}\frac{1}{\tau} + O\left(\frac{\ln^2\tau}{\tau^2}\right)\right], \qquad \tau\to\infty. \tag{2.7}$$

This singular trajectory expansion for $\hat{z}_p$ has the same form as the initial expansion of f, (2.4). And most importantly, the coefficient of the respective temporal order equates to the singularity position of the according asymptotic sublayer. That means, the time-dependent singularity position of the Fisher equation z_p is given in leading order by the singularity position of the initial expansion $\pm\sqrt{8}$, the first order correction will be the singularity position of the first sublayer, and so on.

Starting at $O(1/\tau)$, i.e. at the second sublayer, the motion of the singularity will depend on the introduced integration constants C_i of the initial expansion (2.4). To find for example the connection between the singularity position ζ_s and the initial constant C_1, we need to write down the correct expansions for all layers up to the second sublayer, and merge them together at respective overlap areas using the method of matched asymptotic expansions.

3. The first asymptotic sublayer.

3.1. Temporal expansion. In accordance with the new spatial scaling (2.6) we make the ansatz $f(\hat{z},\tau) = v(\gamma,\tau)$ and insert into the Fisher equation or rather the initial equation (2.3), to obtain the partial differential equation for the first sublayer,

$$\begin{aligned}\frac{\tau}{\ln(\tau)}\left[\sqrt{2}\,\frac{\partial v}{\partial\gamma}+\frac{\partial^2 v}{\partial\gamma^2}\frac{1}{\ln(\tau)}\right]-v^2 = -v-\frac{\gamma}{2}\frac{\partial v}{\partial\gamma}+\sqrt{2}\,\frac{\partial v}{\partial\gamma}\frac{1}{\ln(\tau)}+\\ +\frac{1}{\tau}\left[-\frac{\gamma}{2}\frac{\partial v}{\partial\gamma}+\gamma\,\frac{\partial v}{\partial\gamma}\frac{1}{\ln(\tau)}\right]-\frac{\partial v}{\partial\tau}\,.\end{aligned} \tag{3.1}$$

This equation requires a complicated expansion. To tackle the problem step by step, we introduce $\beta = \ln(\tau)$ and begin with an expansion in complete τ/β-orders only,

$$v(\gamma,\tau) \sim \frac{\tau}{\beta}v_1(\gamma,\beta)+v_2(\gamma,\beta)+O\left(\frac{\beta}{\tau}\right), \qquad \tau\to\infty\,. \tag{3.2}$$

Thereby, we acquire a system of differential equations which is still dependent on β, but in a clear manner,

$$\begin{aligned}&\sqrt{2}\,\frac{\partial v_1}{\partial\gamma}-v_1^2+\frac{\partial^2 v_1}{\partial\gamma^2}\frac{1}{\beta}=0\,,\\ &\sqrt{2}\,\frac{\partial v_2}{\partial\gamma}-2v_1v_2+\frac{\partial^2 v_2}{\partial\gamma^2}\frac{1}{\beta}=-v_1-\frac{\gamma}{2}\frac{\partial v_1}{\partial\gamma}+\sqrt{2}\,\frac{\partial v_1}{\partial\gamma}\frac{1}{\beta}\,,\quad\cdots\,.\end{aligned} \tag{3.3}$$

We can eliminate this remaining temporal dependency through an additional expansion in $\beta\to\infty$, in agreement with $\tau\to\infty$ and $t-t_s\to 0$. This step is not trivial, we actually need to introduce double-logarithmic contributions, i.e. $\ln(\beta)$-terms, in order to make the first sublayer matchable with the initial expansion,

$$v_i(\gamma,\beta) \sim v_{i1}(\gamma)+v_{i2}(\gamma)\frac{\ln(\beta)}{\beta}+v_{i3}(\gamma)\frac{1}{\beta}+O\left(\frac{\ln^2(\beta)}{\beta^2}\right), \qquad \beta\to\infty\,. \tag{3.4}$$

With that we obtain simplified equations of the form

$$\sqrt{2}\,v_{11}'-v_{11}^2=0\,, \qquad \sqrt{2}\,v_{ij}'-2v_{11}v_{ij}=G_{ij}\,. \tag{3.5}$$

Hence, the solution of the leading order v_{11} is simply a first order pole. The inhomogeneity of the linearized higher order equations G_{ij} is zero at the second order and else dependent on solutions v_{ij} of smaller orders. In total we find

$$\begin{aligned}v_1 &\sim -\frac{\sqrt{2}}{a}+\frac{A_{12}}{a^2}\frac{\ln(\beta)}{\beta}+\frac{A_{13}+2\ln|a|}{a^2}\frac{1}{\beta}+\dots\,,\\ v_2 &\sim \frac{A_{21}+A_{11}\gamma+\gamma^2/4}{a^2}+\left[\frac{A_{22}+\frac{A_{12}}{2\sqrt{2}}\gamma}{a^2}+\frac{A_{12}}{2\sqrt{2}}\frac{3A_{11}^2-4A_{21}}{a^3}\right]\frac{\ln(\beta)}{\beta}+\\ &+\left[\frac{\ln|a|}{\sqrt{2}a}+\frac{A_{23}+\frac{A_{13}}{2\sqrt{2}}\gamma}{a^2}+\frac{(3A_{11}^2-4A_{21})(A_{13}-1+2\ln|a|)}{2\sqrt{2}\,a^3}\right]\frac{1}{\beta}+\dots\,,\end{aligned} \tag{3.6}$$

where $a = A_{11} + \gamma$. As common, the pole position is defined through the degree of freedom A_{11} of the leading order function v_{11}.

3.2. Matching and breakdown. We adjust the first sublayer (3.2), i.e. the values of all the introduced constants A_{ij}, to the initial expansion (2.4) using Van Dyke's matching rule, [24]. Hereby, we claim that both expansions are valid in an overlap region $f(\hat{z} \to \sqrt{8}) = v(|\gamma| \to \infty)$, enabling a smooth transition between them and resulting in

$$\begin{aligned} &A_{11} = 1/\sqrt{8}\,, \qquad A_{12} = 2\,, \qquad A_{13} = (2 - C_1)/4 + 5\ln(2)\,, \\ &A_{21} = (1 - 2C_2)/8\,, \qquad A_{22} = 1\,, \qquad A_{23} = (1 - C_3)/4\,. \end{aligned} \tag{3.7}$$

The leading order $O(\tau^0)$ matches automatically. For $O(\tau^{-1})$, $O((\hat{z} - \sqrt{8})^{-2})$ terms proportional to $\ln(\tau)$ match for fixed A_{11}, constant terms for fixed A_{13}, occurring $\ln[\ln(\tau)]$ terms are removed with A_{12}, and $\ln(\hat{z} - \sqrt{8})$ terms match automatically. For more details on the matching, please see appendix A.1.

We readily see, that the expansion of the first sublayer has a singularity at $\gamma = -1/\sqrt{8}$. Thus, we constructed by now the singular trajectory $\hat{z}_p$ (2.7) up to and including $O(\tau/\ln(\tau))$. Without surprise, near this singularity position of γ the first sublayer will collapse, giving rise to a new spatio-temporal area, which we call the second asymptotic sublayer.

In order to find the corresponding breakdown scaling, we follow up the same approach as in subsection 2.2. Since the leading structure of (3.6) is very similar to the initial expansion (2.4), we would obtain $(\gamma + 1/\sqrt{8})\beta/\ln(\beta) \sim O(1)$ as a first result. However, after some studies we actually find that this scaling establishes no correction to the singularity position, i.e. seemingly no new dynamics are hidden within it. Therefore, we consider instead the next possible breakdown of (3.6), associated with the second smallest rescaling. We can define it rudimentarily by the balance between v_{11} and the homogeneous part of v_{13},

$$-\frac{\sqrt{2}}{a} \overset{!}{\sim} \frac{A_{13}}{a^2}\frac{1}{\beta}\,, \tag{3.8}$$

yielding the relevant spatial quantity of the second sublayer, the second inner variable

$$\xi = \left(\gamma + 1/\sqrt{8}\right)\ln(\tau) \sim O(1)\,. \tag{3.9}$$

4. The second sublayer - a numerical challenge.

4.1. Temporal expansion. The next crucial stop on our way to describe the initial singularity motion governed by the Fisher equation is the second asymptotic sublayer. In accordance with the new spatial scaling (3.9) we make the ansatz $v(\gamma, \tau) = w(\xi, \tau)$ and perform this change of variables in the first sublayer equation (3.1), to obtain the partial differential equation of the second sublayer

$$\begin{aligned} \tau\left[\sqrt{2}\,\frac{\partial w}{\partial \xi} + \frac{\partial^2 w}{\partial \xi^2}\right] - w^2 = -w - \frac{\xi}{2}\frac{\partial w}{\partial \xi} + \frac{\beta}{4\sqrt{2}}\frac{\partial w}{\partial \xi} + \sqrt{2}\,\frac{\partial w}{\partial \xi} + \\ + \frac{1}{\tau}\left[-\frac{\xi}{2}\frac{\partial w}{\partial \xi} + \frac{\beta}{4\sqrt{2}}\frac{\partial w}{\partial \xi} - \frac{1}{2\sqrt{2}}\frac{\partial w}{\partial \xi}\right] - \frac{\partial w}{\partial \tau}\,. \end{aligned} \tag{4.1}$$

In order to avoid unnecessary prefactors, we implement an additional linear transformation $w(\xi,\tau) = 2g(\zeta,\tau)$ with $\zeta = \sqrt{2}\,\xi$. In accordance, the correct asymptotic expansion of g is given by

$$g(\zeta,\tau) \sim \tau g_1(\zeta) + \left[\beta^2 g_2(\zeta) + \beta g_3(\zeta) + g_4(\zeta)\right] + O(\beta^4/\tau), \qquad \tau \to \infty\,. \tag{4.2}$$

Similar as in section 3, we again had to introduce additional orders starting with g_2, such that the matching with the first sublayer is possible. In particular, the second temporal order in each layer is pictured through a homogeneous equation. This degeneration gets imprinted onto the sublayers from the initial expansion (2.4). We insert expansion (4.2) into (4.1) and obtain the equations for $g_j(\zeta)$,

$$g_1'' + g_1' = g_1^2\,, \qquad g_i'' + g_i' - 2g_1 g_i = G_i\,, \qquad i = 2,3,\dots\,, \tag{4.3}$$

where G_i corresponds to the inhomogeneity of the respective higher order. We see, the leading order equation inherits finally a full balance between the second and first derivative and the nonlinearity. Hence, g_1 is seemingly no longer analytically determinable and we focus on its numerical computation. For the sake of completeness, we note that the equation for g_1 describes a singular traveling wave of (1.1) in the limit of infinite wave speeds $c \to \infty$, as suggested by the representation $u(z,t) = c^2 g_1(\zeta)$ and the appropriate wave variable $\zeta = c(z-ct) - \zeta_0$, [3].

4.2. Properties of the leading order. Let us consider the relevant asymptotic behavior of g_1, derived from equation (4.3),

$$g_1 \sim \begin{cases} -\dfrac{1}{\zeta} + \dfrac{\ln(\zeta^2)}{\zeta^2} + \dfrac{F_1}{\zeta^2} + o(\zeta^{-2})\,, & \zeta \to \pm\infty\,, \\[2ex] \dfrac{6}{(\zeta-\zeta_s)^2} - \dfrac{6/5}{\zeta-\zeta_s} - \dfrac{1}{50} + O(\zeta-\zeta_s)\,, & \zeta - \zeta_s \to 0^{\pm}\,. \end{cases} \tag{4.4}$$

On the one hand, we have written down the expansion of the far field for $\zeta \to \pm\infty$, where logarithmic contributions appear and the far field constant F_1 gets introduced. And on the other hand, we formulated the expansion around the expected but yet unknown singularity position of the second sublayer, $\zeta - \zeta_s \to 0$, which we call the near field of g_1. We see that the singularity is a combination of a pole of second and first order.

The far field constant F_1 gets its variable value imprinted from the matching with the first sublayer $v(\gamma \to -1/\sqrt{8}) = 2g(|\zeta| \to \infty)$, yielding

$$F_1 = A_{13} - \ln(2) = (2 - C_1)/4 + 4\ln(2)\,. \tag{4.5}$$

But most importantly, F_1 takes the same value at both far field areas, which fixes one degree of freedom of the equation. The other degree of freedom of the leading order function is its invariance under position shifts. The choice of the singularity position ζ_s breaks this translation invariance, i.e. ζ_s is the second degree of freedom.

Using this knowledge we can simply shift the singularity position ζ_s to the origin $\zeta \to \zeta - \zeta_s$ and track the corresponding changes in F_1, in order to obtain the desired relation between these two constants (see also appendix A.2),

$$F_1 + \zeta_s = M = const\,. \tag{4.6}$$

A quite remarkable result, while the transition from the partially logarithmic far field contributions towards the algebraic near field terms is fully nonlinear, the actual position of the singularity is linearly dependent on the far field constant. The remaining constant M is the missing quantity, we need to calculate its value within the numerical scheme.

4.3. Computation with spectral collocation. In order to compute g_1 we need to separate some hindering terms. Due to the asymptotic structure (4.4) an additive separation seems to be best suited,

$$g_1(\zeta) = h(\zeta) + \frac{6}{(\zeta-\zeta_s)^2} - \frac{6/5}{\zeta-\zeta_s} + \frac{(\zeta-\zeta_s)/5}{(\zeta-\zeta_s)^2+1} + \frac{\ln\left[(\zeta-\zeta_s)^2+1\right]}{(\zeta-\zeta_s)^2+1}\,. \tag{4.7}$$

Here, the first two separation terms eliminate the singularity, to generate a bounded solution for the auxiliary function $h(\zeta)$. And with the last two terms we remove the first two far field terms in (4.4), in order to get access to F_1, or rather M. The remaining function h is then indeed numerically determinable, the regarding asymptotic representations simplify to

$$h(\zeta) \sim \begin{cases} \dfrac{M-6}{\zeta^2} + o(\zeta^{-2})\,, & \zeta \to \pm\infty\,, \\ -1/50 + O(\zeta-\zeta_s)\,, & \zeta-\zeta_s \to 0^{\pm}\,. \end{cases} \tag{4.8}$$

For the numerical method we have chosen Chebyshev pseudo spectral collocation, the according differentiation matrices $D_{ij}^{(k)}$ of order k are defined on the Gauss–Lobatto points ($N+1$ collocation points $s_i = -\cos(\pi i/N)$, $i,j \in [0,N]$), [23, 6, 1]. Hence, we transform the infinite spatial domain $\zeta \in (-\infty,\infty)$ to the bounded Chebyshev domain $s \in [-1,1]$ using the mapping

$$\zeta(s) = B\tan(\pi s/2) + \zeta_s\,, \tag{4.9}$$

where we placed the singularity at $s=0$ and B takes the role of a stretching parameter. The smaller B, the denser is the grid around ζ_s. Then, the differentiation matrices in the ζ-domain $\mathcal{D}_{ij}^{(k)}$ are given by the product rule,

$$\mathcal{D}_{ij}^{(1)} = \frac{\mathrm{d}s}{\mathrm{d}\zeta} D_{ij}^{(1)}\,, \qquad \mathcal{D}_{ij}^{(2)} = \frac{\mathrm{d}^2 s}{\mathrm{d}\zeta^2} D_{ij}^{(1)} + \left(\frac{\mathrm{d}s}{\mathrm{d}\zeta}\right)^2 D_{ij}^{(2)}\,. \tag{4.10}$$

The domain mapping (4.9) is very practical for us, it enables a direct access to $M = F_1 + \zeta_s$ in (4.8) through the second s-derivative at the system boundaries,

$$\frac{\mathrm{d}^2 h}{\mathrm{d}s^2}(s=\pm 1) = \frac{\pi^2}{2B^2}\,(M-6)\,. \tag{4.11}$$

Now we can finally formulate proper boundary/interior conditions for the leading order equation, namely

$$h(s=0) = -\frac{1}{50}\,, \qquad \frac{\mathrm{d}h}{\mathrm{d}s}(s=\pm 1) = 0\,, \qquad \left.\frac{\mathrm{d}^2 h}{\mathrm{d}s^2}\right|_{s=-1}^{1} = 0\,. \tag{4.12}$$

The last condition equates the second derivative on the left and right boundary to each other, i.e. it makes sure that the two far field areas $\zeta \to \pm\infty$ take the same (still unknown) value of F_1. The first condition yields the function value at the singularity position (where the differential equation can not be evaluated numerically). The remaining conditions are only imposed to enhance numerical convergence.

With this approach we managed to solve the boundary value problem (4.3) for g_1. The resulting functional behaviour of $h(s)$, after the separation (4.7), is visualised in figure 2A. Additionally, we plotted g_1 in dependence of ζ without its poles in figure

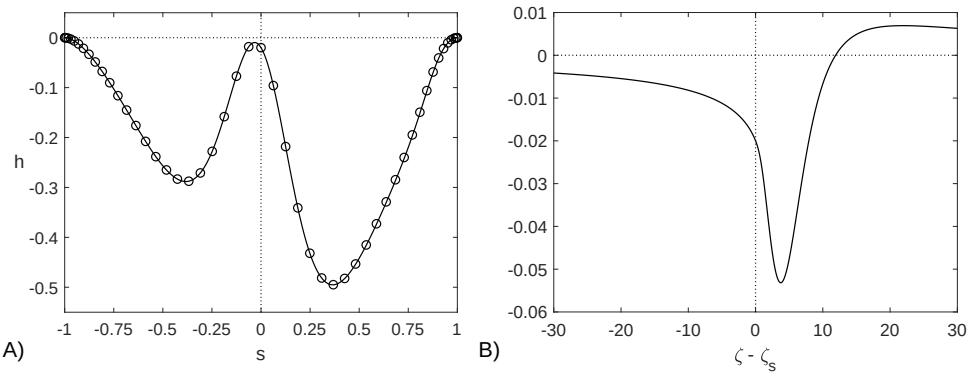

FIG. 2. *Solution of the leading order equation of the second sublayer* (4.3). *A) Numerical solution of h,* (A.4)*, on the Chebyshev grid s (circles), according to the mapping* (4.9) *with* $B = 2$ *and* $N = 50$ *collocation points. B) Finite part of* g_1 *(i.e. modulo its pole structure) in dependence of the second inner variable* ζ*,* (3.9).

2B. Besides in the far field, the first order function is almost solely given by the singularity as a combination of second and first order poles.

After the computation we conveniently read out the missing constant M from the second derivative (4.11) and find

$$M = F_1 + \zeta_s \approx -0.0566\,. \tag{4.13}$$

Due to the remaining logarithmic contributions hidden in the higher orders of the far field, which can not be resolved precisely by the interpolated Chebyshev polynomials, the numerical solution is spurious to some extent. Hence, we performed the computation with a rising number of grid points N until $N = 900$ and observed the convergence of M towards the slightly negative estimate provided above (see table 1 in appendix A.2).

We track F_1 back to the initial constant C_1 with (4.5), yielding the relation to the singularity position of the second sublayer,

$$\zeta_s = (C_1 - 2)/4 + M - 4\ln(2)\,. \tag{4.14}$$

Based on the solution of the leading order equation, we can compute the higher orders g_j in (4.1) with similar approaches (up to a point, where the resolution of the leading order is no longer sufficient) and estimate further relations between constants (to be found in the appendix A.2).

5. Final results and outlook.

5.1. The singular trajectory expansion. We start with some final comments regarding the expansions with respect to the exponentially short time scale τ. During each zooming process the second derivative rises stronger then the first derivative. The initial expansion and the first layer are dominated by the balance between the first spatial derivative and the nonlinearity. At the level of the second sublayer occurs the threefold balance, as the second derivative joins in. The leading order $l_i = l(\mu_i)$ of each subsequent layer after the second will be determined through a balance between

the second derivative and the nonlinearity solely,

$$l'' = l^2 \qquad \Rightarrow \qquad l_i = 6/(\mu_i - D_i)^2 \,. \tag{5.1}$$

The general solution of this equation is known in literature as the Weierstrass elliptic $\wp$-function, $l(\mu_i) = 6^{1/3}\wp\left(6^{-1/3}(\mu_i - D_i); g_2 = 0, g_3\right)$, [7, Eq. 23.3.12]. However, the matching between layers requires a well defined far field and thus a non-periodic solution (which requires the specific value of the lattice invariant $g_3 = 0$), yielding that l_i is always fixed to a pure pole of second order, positioned at some location D_i. For this reason, the essential dynamics of the singularity motion is inherited in the first two sublayers.

Actually, we find that the asymptotic solution of each subsequent layer (starting with the near field of the second sublayer) is simply given by a singular traveling wave solution of the Fisher equation (1.1),

$$u \sim \frac{6}{[z - z_p(t)]^2} - \frac{6/5}{[z - z_p(t)]}\frac{\mathrm{d}z_p}{\mathrm{d}t} + \left[\frac{1}{2} - \frac{1}{50}\left(\frac{\mathrm{d}z_p}{\mathrm{d}t}\right)^2\right] + \dots \,, \quad z - z_p(t) \to 0^{\pm} \,, \tag{5.2}$$

where the singularity motion $z_p(t)$ is the sole characteristic quantity. The complicated dynamics of the first two sublayers (relevant near the initial blow-up point) simplifies smoothly to a singular traveling wave! The structure of any layer after the second can easily be verified through performing the change of variables in (5.2) to the respective spatial coordinate μ_i (see appendix A.3).

The initial motion of the Fisher singularity pair $z_p(t)$ is given by the singular trajectory expansion for $\tau = -\ln|t - t_s| \to \infty$,

$$\frac{z_p - z_s}{\pm\sqrt{8\tau(t - t_s)}} \sim 1 - \frac{1}{8}\frac{\ln(\tau)}{\tau} + \frac{\zeta_s}{4}\frac{1}{\tau} + \eta_s\frac{\ln^2(\tau)}{\tau^2} + \delta_s\frac{\ln(\tau)}{\tau^2} + \frac{\mu_s}{\tau^2} + \dots \,. \tag{5.3}$$

Each temporal order τ^{-n} (including the $\ln(\tau)$-contributions) splits up into $n + 1$ distinct terms and is determined by n degrees of freedom C_i of the initial expansion (2.4). We tracked the first appearing constant ζ_s back to the initial constant C_1, resulting in the relation (4.14). The same can be done for the other entries. The more complicated relations of the second temporal order get partially worked out in appendix A.

Afterwards, one could theoretically fit the initial expansion (2.4), i.e. the constants C_i, to a numerical solution of the Fisher equation (1.1) shortly before the point blow-up occurs and determine the corresponding initial motion of the singularities after the blow-up. Of course, due to the involvement of the exponentially short time scale τ, this numerical matching process is rather difficult to achieve.

Instead we study the general form of (5.3) in order to search for a temporal limit and to compare it with some numerical results known from literature. For this sake we visualised in figure 3A the time dependency of the different orders in (5.3) (with all coefficients set to 1). Then, we see that the ordering of some terms changes at distinct times $\tau = e$ and $\tau = 1$. While the first change is seemingly harmless, the expansion will surely break down at $\tau = 1$, where the $\ln(\tau)$ contributions vanish and the remaining complete orders τ^n are all of the same magnitude. Needless to say, in general the coefficients will modulate the breakdown time to some τ_{fin}.

Since we expect a distinct change after this exponentially short time scale regime, such an above-described complete breakdown seems reasonable. In accordance the

magnitudes of the complete orders get fixed to $(\tau_{fin}/\tau)^n$, but actually no restrictions on the $\ln(\tau)$-terms get imposed. In addition, we obviously want to consider that the expansion converges at all times $\tau \in (\infty, \tau_{fin})$, making an alternating series a very appealing candidate.

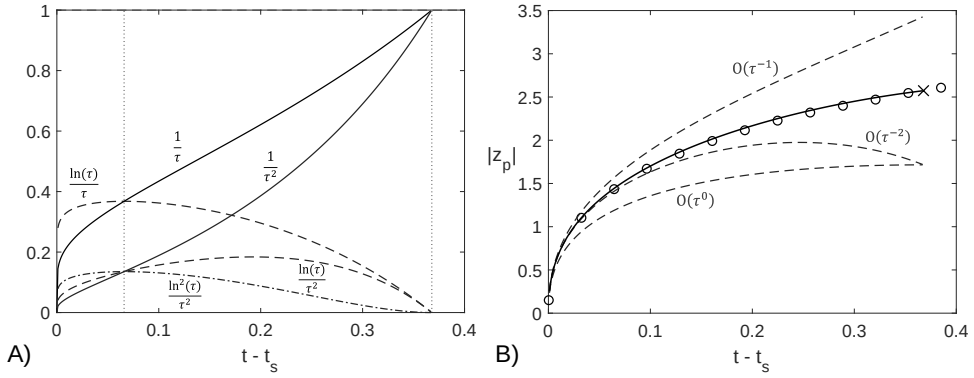

FIG. 3. *Temporal behaviour of the singular trajectory expansion* (5.3). *A) Plot of the different temporal orders up to* τ^{-2}. *The* $\ln(\tau)$*-contributions (dashed lines) vanish at* $\tau = 1$, *i.e.* $t - t_s = e^{-1}$. *B) Comparison of our estimate* (5.7) *(solid line) with the numerical values from Weideman [25] (empty circles) and the temporal limit* (5.6) *(cross). In addition, we pictured some partial sums (dashed lines).*

5.2. Comparison to complex valued singularities. We keep the last paragraph in mind, while we start to compare the singular trajectory expansion (5.3) to some literature values of the singularity motion. Before the blow-up occurs at t_s the singularity pair exist already in the complex plane, here the propagation of the singularities towards the real axis can actually be tracked numerically with the methods of complex analysis. The thereby determined trajectory shortly before t_s is of relevance for us, since it is related to the initial motion beyond t_s through a simple symmetry consideration. As already mentioned in the introduction, near the point blow-up $t - t_s \to 0^{\pm}$ the Fisher equation (1.1) satisfies asymptotically

$$\frac{\partial u}{\partial t} - \frac{\partial^2 u}{\partial z^2} \sim -u^2 \qquad \Rightarrow \qquad u(z - z_s, t - t_s) \sim -u\big(i(z - z_s), t_s - t\big)\,. \tag{5.4}$$

The initial expansion (2.4) is an example of this invariance. Therefore, we can compare our results with the numerical findings obtained by Weideman [25] in figure 3B, who computed the motion of complex singularities before blow-up. Since everything happens on a very short time scale, there are too few data points near $\tau \to \infty$ to fit the constants in the singular trajectory expansion (5.3) appropriately. Thus, we make some additional guesses to obtain a convergent expansion. We set $\tau_{fin} = 1$ and assume a geometric series in the complete τ-orders,

$$\frac{z_p - z_s}{\pm\sqrt{8\tau(t - t_s)}} \sim 2 - \sum_{n=0}^{\infty}\left(-\frac{1}{\tau}\right)^n - \frac{1}{8}\frac{\ln(\tau)}{\tau} + \ldots = \frac{1}{1+\tau} + 1 - \frac{1}{8}\frac{\ln(\tau)}{\tau} + \ldots\,. \tag{5.5}$$

In agreement with the anticipated complete breakdown at $t_{fin} - t_s = e^{-1}$, there are no restrictions on the $\ln(\tau)$-contributions. Nevertheless, the series limit at t_{fin} is anyway

independent from them and takes the value

$$z_p(t_{fin}) - z_s = 3\sqrt{2/e}\,, \tag{5.6}$$

which fits very well to the data points in figure 3B. For the sake of comparison, we tried also to fix the $\ln(\tau)$-contributions using a similar approach, resulting in an imperfect analytical estimate

$$\frac{z_p - z_s}{\pm\sqrt{8\tau(t-t_s)}} \approx 1 + \frac{1}{1+\tau}\left(1 - \frac{1}{8}\frac{\tau\ln(\tau)}{\tau - \ln(\tau)}\right). \tag{5.7}$$

Overall, our estimate is in good agreement for $\tau \to \infty$ as well as near $\tau_{fin} = 1$. We believe, the minor discrepancies in interim times might be removable through appropriate modulation of the $\ln(\tau)$-terms solely.

The general breakdown of the singular trajectory expansion at some τ_{fin} naturally rises the question of what to expect after this initial temporal phase. So far we don't know how to extend our solution appropriately to later times. One possibility might be a local Taylor expansion of the initial equation for f, (2.3), around τ_{fin} and $\hat{z}_p(\tau_{fin})$, without a scaling change, and to get rid of the explicit τ-dependencies afterwards. In such a way, that the solution is still given locally by a singular traveling wave with a time-dependent wave speed (5.2).

The final long-term goal would be a time-dependent separation of the singularity structure, in order to compute the remaining finite part of the solution numerically. And as a further step, the regularization of the mentioned breakdown of interaction boundary layer theory (see appendix B), through additional spatio-temporal stages, such that we can resolve more details of the vortex generation process and the associated, incipient laminar-turbulent transition in general.

6. Conclusions. In summary, we introduced the forced Fisher–KPP equation (1.1) as the most simplified evolution equation for lambda and hairpin type vortex generation processes in its essence. Here, the vicinity of singular points of the solution u depicts the areas of large vorticity (wall shear stress). We were able to describe the singularity motion and the occurring complicated changes in the singularity structure beyond the initial blow-up of u with the method of matched asymptotic expansions.

The singularities change smoothly from a pole of first order at the blow-up time towards a pole of second order. We encrypted this transition process through the first two asymptotic sublayers. The resulting singular trajectory expansion describes the initial motion of the Fisher singularity pair beyond finite-time blow-up and our investigations even indicate that the pure singularity can be described as a singular traveling wave with a time-dependent propagation speed. Thus, the creation (2.4), motion (5.3), and structure (5.2) of the singularities is bound to some form of symmetry of the underlying equation (1.1).

We believe that our results give an much-anticipated, alternative insight into the nonlinear motion of singularities of reaction-diffusion type equations (aka semilinear heat equations), as well as in the general handling of logarithmic terms in singular perturbation problems. Such logarithmic contributions appear temporally through the time scales τ and $\beta = \ln\tau$, but also spatially, e.g. in the far field of the second sublayer. Here, the computation of the leading order equation for g_1, (4.3), is of special relevance. The threefold balance between the second and first derivative and the quadratic nonlinearity enables a transition from logarithmic far field contributions towards an algebraic near field.

Appendix A. Blow-up expansions. We derive additional orders of the singular trajectory expansion up to $O\left(\tau^{-2}\right)$, accompanied with some comments to matching and numerics.

A.1. Matching with the initial expansion. The next higher order terms for f in the initial expansion (2.4) are

$$\begin{aligned} f \sim \ldots \mp \hat{z}^2 \left[\frac{C_2}{a^2} - \frac{100}{a^3}\right] \frac{\ln^2 \tau}{\tau^2} + \left[\frac{20 \mp C_3 \hat{z}^2}{a^2} \mp 20 \hat{z}^2 \frac{2 + C_1 - 8 \ln|a|}{a^3}\right] \frac{\ln \tau}{\tau^2} + \\ + \left[-\frac{9 + C_1/4 - 2\ln|a|}{a} - \frac{24 \pm C_3 \hat{z}^2 - b}{a^2} + 8 \frac{84 - b \pm 8\hat{z}^2 \ln^2|a|}{a^3}\right] \frac{1}{\tau^2} + \ldots , \end{aligned} \tag{A.1}$$

where we have used the abbreviations $a = 8 \mp \hat{z}^2$ and $b = 16(2+C_1)\ln|a| - C_1(4+C_1)$ and the constants C_2 and C_3 appear. Their main contributions to the first sublayer are already written down in (3.7), some further matching relations are

$$\begin{aligned} &A_{14} = A_{15} = A_{16} = 0\,, \quad A_{24} = -1\,, \quad A_{25} = (C_1 - 6)/4 - 4\ln(2)\,, \\ &A_{26} = (47 + 3C_1)/16 - C_1^2/64 - C_3/2 + (C_1 - 6)\ln(2)/2 - 4\ln^2(2)\,. \end{aligned} \tag{A.2}$$

We obtain them from the matching rule $f(\hat{z} \to \sqrt{8}) = v(|\gamma| \to \infty)$. Where we first expand the two functions around the respective spatial coordinate value (the near field of f corresponds to the far field of v) and afterwards we express v with respect to $\hat{z}$, using (2.6), in order to compare the different spatio-temporal orders.

In this context, the two expansion match in the leading orders $[O(1), O(1/\tau)] \times \left[O((\hat{z} \mp \sqrt{8})^{-2}), O((\hat{z} \mp \sqrt{8})^{-1})\right]$ for the determined values of A_{1j}. In particular, at $O(1/\tau)$, $O((\hat{z} \mp \sqrt{8})^{-1})$ terms from v_2 (3.6) make first contributions, but no additional constants appear. The values of $A_{21} - A_{26}$ get determined through the spatial order $O((\hat{z} \mp \sqrt{8})^{-2})$ in $O(1/\tau^2)$, we believe this pattern will be continued for the subsequent temporal orders.

A little bit bothersome is the breakdown near the singularity of the first sublayer. The supposed first breakdown scaling turned out irrelevant, since no shift in the pole position gets introduced with it. We want to mention that this could change if for some reason additional $\ln[\ln(\tau)]$-contributions are present in the initial expansion (2.4). Such terms would be only relevant shortly before and beyond the blow-up, and might therefore not be resolvable/desirable. So far we see no indication for them, hence we continue with the second smallest scaling change (3.9) and arrive at the second sublayer.

A.2. Computation of the second sublayer. For a quick verification of the linear connection between F_1 and ζ_s, eq. (4.6), we perform the coordinate shift $\zeta \to \zeta_* = \zeta - \zeta_s$, such that $\zeta_{*s} = 0$. Then, the far field (4.4) changes to

$$g_1 \sim -\frac{1}{\zeta_*} + \frac{\ln(\zeta_*^2)}{\zeta_*^2} + \frac{F_1(\zeta_s) + \zeta_s}{\zeta_*^2} + o(\zeta_*^{-2})\,, \qquad \zeta_* \to \infty\,, \tag{A.3}$$

yielding $F_1(0) = F_1(\zeta_s) + \zeta_s = M$. The first order of $g_1(\zeta \to \infty)$ contributes to the second order of $g_1(\zeta_* \to \infty)$, this also explains why M appears naturally in (4.8).

The leading order equation of the second sublayer for g_1 (4.3) takes after the

separation ansatz (4.7) the following nonlinear form

$$
\begin{aligned}
h''+h'-\left[h+\frac{12}{\zeta^2}-\frac{12}{5\zeta}+\frac{2\zeta/5+2\ln(a)}{a}\right]h = \\
=\left[\frac{12}{5\zeta}-\frac{17}{25}+\left(\frac{12}{\zeta^2}-\frac{12}{5\zeta}\right)\ln(a)\right]\frac{1}{a}-\left[\frac{8}{5}\zeta-12+8\ln(a)\right]\frac{\zeta^2}{a^3}+ \\
+\left[\frac{11}{25}\zeta^2-\frac{4}{5}\zeta-2+\left(\frac{12}{5}\zeta+2\right)\ln(a)+\ln^2(a)\right]\frac{1}{a^2}+\frac{6/25}{\zeta^2}\,,
\end{aligned}
\tag{A.4}
$$

with $a=\zeta^2+1$ and $\zeta_s=0$ (for the general form shift $\zeta\to\zeta-\zeta_s$). We achieved a numerical solution of this equation using Chebyshev collocation (see subsection 4.3), the corresponding behaviour of h on both, the Chebyshev and physical domains s and ζ, is visualised in figures 4, 5A.

Since the far field gets not approximated precisely, we computed h with an increasing number of grid points N. While the overall solution behaviour does not change with N, the important constant M, (4.13), converges only slowly, listed in table 1. A resolution much greater than $N=900$ is not reasonable, as the large mode coefficients are already of magnitude $\sim 10^{-15}$, i.e. near the machine precision.

TABLE 1

Values of $M=F_1+\zeta_s$, (4.13), in dependence of the number of collocation points N for $B=4$. Extrapolation estimates for $N\to\infty$ yield $M\approx -0.0567$ or $M\approx -0.0569$ based on the assumption of exponential or algebraic convergence, respectively.

N_i	100	200	400	600	800	900
M_i	-0.0382	-0.0511	-0.0553	-0.0562	-0.0565	-0.0566
M_{i+1}/M_i-1	0.3382	0.0813	0.0158	0.0058	0.0016	—

In order to get more trust in our result we compare in figure 4 the numerical solution of g_1 after separation (4.7) with the far field expansion as $\zeta\to\pm\infty$,

$$
h\sim\frac{M-6}{\zeta^2}-\frac{\ln^2(\zeta^2)}{\zeta^3}-2(M-1)\frac{\ln(\zeta^2)}{\zeta^3}-\frac{(M-1)^2+24/5}{\zeta^3}+o(\zeta^{-3})\,.
\tag{A.5}
$$

We see that not only the leading order of the expansion, but also the subsequent logarithmic and M-dependent terms, get resolved conveniently by our numerical solution.

The next three orders of the second sublayer expansion (4.2) satisfy

$$
\begin{aligned}
g_2''+g_2'-2g_1g_2=0\,,\qquad g_3''+g_3'-2g_1g_3=g_1'/8\,,\\
g_4''+g_4'-2g_1g_4=(1-\zeta/4)\,g_1'-g_1/2\,.
\end{aligned}
\tag{A.6}
$$

Their far field behaviour as $\zeta\to\pm\infty$ is again defined by far field constants F_i, which get always introduced at order ζ^{-2} (in the upcoming expansions of g_i). The singularity position ζ_s gets imprinted from the leading order g_1. Then, the matching with the first sublayer yields

$$
F_2=(1/8-C_2)/4,\quad F_3=(1-C_3)/4\,,\quad F_4=F_3-(F_1+1)^2/8+3/2\,,
\tag{A.7}
$$

where F_4 inherits no additional degree of freedom.

To formulate the associated boundary value problems and to solve them numerically we follow the approach of subsection 4.3. We start with g_2 and its relevant

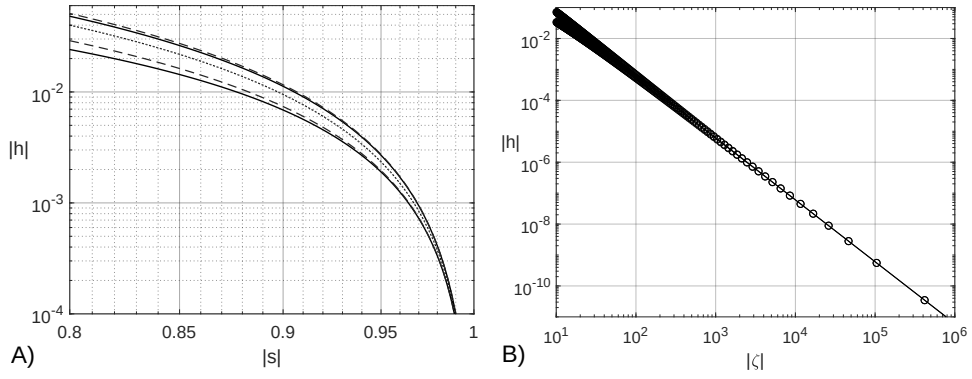

FIG. 4. *Comparison of our numerical solution $|h|$ with the far field asymptotics* (A.5) *(upper branch $\zeta \to \infty$, lower branch $\zeta \to -\infty$). We used the outcomes of the highest resolution $N = 900$ with $B = 4$, and the estimated constant $M \approx -0.0566$. A) $h(s)$ (solid line) and asymptotics up to $O(\zeta^{-2})$ (dotted line) as well as up to $O(\zeta^{-3})$ (dashed line). B) Log-Log plot of $h(\zeta \to \pm\infty)$, the solution (empty circles) is nearly indistinguishable from the asymptotic representation (solid line).*

asymptotic expansions, near the far field and near ζ_s,

$$g_2 \sim \begin{cases} F_2 \left[\dfrac{1}{\zeta^2} - \dfrac{2\ln^2(\zeta^2) + 2(F_1 - 1)}{\zeta^3} + o(\zeta^{-3}) \right], & \zeta \to \pm\infty\,, \\ D_2 \left[\dfrac{1}{(\zeta - \zeta_s)^3} - \dfrac{1/10}{(\zeta - \zeta_s)^2} + \dfrac{1}{3000} + O(\zeta - \zeta_s) \right], & \zeta - \zeta_s \to 0^{\pm}\,. \end{cases} \tag{A.8}$$

The linear eq. (A.6) for the second order has two intrinsic degrees of freedom, namely the scaling invariance denoted by D_2 and the difference between the two far field constants, which is in our case anyway set to zero through matching. In addition, the translation invariance of the singularity ζ_s gets imprinted by g_1 (and automatically resolved through F_1, the other constants F_2 and D_2 are invariant under ζ_s-shifts).

In order to eliminate the scaling invariance, we simply scale $g_2 \to D_2 g_2$ (or equivalently set $D_2 = 1$). Again only an additive separation of the singular contributions is thinkable, such that we define the bounded function $f_2(\zeta)$ through

$$g_2(\zeta) = f_2(\zeta) + \frac{1}{(\zeta - \zeta_s)^3} - \frac{1/10}{(\zeta - \zeta_s)^2}\,, \tag{A.9}$$

with asymptotic structure

$$f_2 \sim \begin{cases} \dfrac{1}{\zeta^2}\left(\dfrac{F_2}{D_2} + \dfrac{1}{10}\right) + o(\zeta^{-2})\,, & \zeta \to \pm\infty\,, \\ 1/3000 + O(\zeta - \zeta_s)\,, & \zeta - \zeta_s \to 0^{\pm}\,. \end{cases} \tag{A.10}$$

We apply the domain mapping (4.9) and obtain access to the scaling constant F_2/D_2 via the second s-derivative of f_2,

$$\frac{F_2}{D_2} = \frac{2B^2}{\pi^2}\frac{\mathrm{d}^2 f_2}{\mathrm{d}s^2}(s = \pm 1) - \frac{1}{10}\,. \tag{A.11}$$

Hence, appropriate boundary conditions are given by

$$f_2(s=0) = \frac{1}{3000}\,, \qquad \frac{\mathrm{d}f_2}{\mathrm{d}s}(s=\pm 1) = 0\,, \qquad \frac{\mathrm{d}^2 f_2}{\mathrm{d}s^2}\Big|_{s=-1}^{1} = 0\,. \tag{A.12}$$

According results of the computation with Chebyshev collocation are visualised in figure 5B, using (A.11) we find the surprisingly simple result

$$F_2/D_2 \approx -0.083336 \approx -1/12\,. \tag{A.13}$$

We continue with the discussion of the next order function g_3 in (A.6). The relevant asymptotic representations are

$$g_3 \sim \begin{cases} \dfrac{1/8}{\zeta} + \dfrac{F_3}{\zeta^2} + o(\zeta^{-2})\,, & \zeta \to \pm\infty\,, \\ \dfrac{D_3}{(\zeta-\zeta_s)^3} - \dfrac{D_3/10}{(\zeta-\zeta_s)^2} + \dfrac{3/20}{(\zeta-\zeta_s)} + \dfrac{D_3}{3000} + \dfrac{1}{200}\,, & \zeta-\zeta_s \to 0^{\pm}\,. \end{cases} \tag{A.14}$$

Since the solution of the homogeneous part of all higher order equations is given by g_2, we only need to search for a special solution (with levelled far field constants). Thus, we choose the special solution $g_{3,s}$ with $D_{3,s} = 0$ and we accordingly split the far field constant into a homogeneous and a particular part $F_3 = F_{3,h} + F_{3,s}$. We separate the remaining first order pole and the first far field term, to get access to the invariant constant,

$$g_{3,s}(\zeta) = f_3(\zeta) + \frac{3/20}{(\zeta-\zeta_s)} - \frac{(\zeta-\zeta_s)/40}{(\zeta-\zeta_s)^2+1}\,. \tag{A.15}$$

In correspondence the bounded function f_3 has the following asymptotic structure

$$f_3 \sim \begin{cases} \dfrac{F_{3,s} - \zeta_s/8}{\zeta^2} + o(\zeta^{-2})\,, & \zeta \to \pm\infty\,, \\ 1/200 + O(\zeta-\zeta_s)\,, & \zeta-\zeta_s \to 0^{\pm}\,. \end{cases} \tag{A.16}$$

As before, we use the spatial mapping (4.9) and appropriate boundary/interior conditions are

$$f_3(s=0) = \frac{1}{200}\,, \qquad \frac{\mathrm{d}f_3}{\mathrm{d}s}(s=\pm 1) = 0\,, \qquad \frac{\mathrm{d}^2 f_3}{\mathrm{d}s^2}\Big|_{s=-1}^{1} = 0\,. \tag{A.17}$$

The constant $\mathcal{F}_{3,s} - \zeta_s/8$ is again connected to the second s-derivative at the boundary, such that the relation between far and near field is depicted through

$$F_3 = F_{3,h} + F_{3,s} = -\frac{D_3}{12} + \frac{\zeta_s}{8} + \frac{2B^2}{\pi^2}\frac{\mathrm{d}^2 f_3}{\mathrm{d}s^2}(s=\pm 1)\,. \tag{A.18}$$

To stay consistent in the calculation of g_1' in the differential equation for g_3 (or rather f_3), we take the numerical derivative of h_1 and add up the analytical terms according to the separation ansatz (4.7). The numerical solution is visualised in figure 5C, where f_3 and its spatial derivatives are plotted. Thereby, we obtain the simple value

$$F_{3,s} - \frac{\zeta_s}{8} = \frac{2B^2}{\pi^2}\frac{\mathrm{d}^2 f_3}{\mathrm{d}s^2}(s=\pm 1) \approx -0.24995 \approx -\frac{1}{4}\,. \tag{A.19}$$

The last example we want to consider is the differential equation for the forth order g_4, stated in (A.6). In contrast to the before discussed orders, g_4 is not invariant under ζ_s-shifts. Hence, we can not immediately determine how the appearing far field constant F_4 depends on the singularity position ζ_s. In order to bypass this problem, we try to work instead with an appropriate linear combination of g_3 and g_4,

$$g_n(\zeta) := 2(\zeta_s - 4)g_3(\zeta) + g_4(\zeta)\,, \tag{A.20}$$

generating a ζ_s-translation invariant equation for $g_n(\zeta)$,

$$g_n'' + g_n' - 2g_1 g_n = -(\zeta - \zeta_s)g_1'/4 - g_1/2\,. \tag{A.21}$$

Naturally, the far and the near field constant transforms correspondingly,

$$F_n = 2(\zeta_s - 4)F_3 + F_4\,, \quad D_n = 2(\zeta_s - 4)D_3 + D_4\,. \tag{A.22}$$

Here, the scenario $\zeta_s = 4$ is seemingly special. It fits to the choice we made in our analytical estimate (5.7) of the singular trajectory. Currently, we do not know if this is pure coincidence or if ζ_s is actually always fixed to this certain value.

The relevant expansions of $g_n(\zeta)$ are given by

$$g_n \sim \begin{cases} \dfrac{1}{8} + \dfrac{\ln(\zeta^2)}{4\zeta} + \dfrac{F_1 + \zeta_s - 4}{4\zeta} - \dfrac{1}{8}\dfrac{\ln^2(\zeta^2)}{\zeta^2} - \dfrac{F_1 + 1}{4}\dfrac{\ln(\zeta^2)}{\zeta^2} + \dfrac{F_n}{\zeta^2}, & \zeta \to \pm\infty\,, \\ D_n\left(\dfrac{1}{(\zeta - \zeta_s)^3} - \dfrac{1/10}{(\zeta - \zeta_s)^2} + \dfrac{1}{3000}\right) - \dfrac{\zeta - \zeta_s}{40}\,, & \zeta - \zeta_s \to 0^{\pm}\,. \end{cases} \tag{A.23}$$

We again only need to find a special solution $g_{n,s}(\zeta)$, where we set $D_{n,s} = 0$. Despite the fact that $g_{n,s}$ is already regular, we still need to separate far field contributions to get access to $\mathcal{F}_{n,s}$. Thus, we try to additively eliminate all far field terms before the constant,

$$g_{n,s}(\zeta) = f_n(\zeta) + \frac{1}{8} + (\zeta - \zeta_s)\frac{\ln(b) + M - 4}{4b} - \frac{1}{8}\frac{\ln^2(b)}{b} - \frac{M+1}{4}\frac{\ln(b)}{b}\,, \tag{A.24}$$

where $b(\zeta) = 1 + (\zeta - \zeta_s)^2$. Then, the asymptotic expansions simplify to

$$f_n \sim \begin{cases} \dfrac{F_{n,s} - \zeta_s(M-6)/4}{\zeta^2} + o(\zeta^{-2})\,, & \zeta \to \pm\infty\,, \\ -1/8 + O(\zeta - \zeta_s)\,, & \zeta - \zeta_s \to 0^{\pm}\,. \end{cases} \tag{A.25}$$

Sadly, due to the lengthy and M-dependent separation, the according numerical solution of f_n, visualised in figure 5D, is too imprecise for a reliable determination of the invariant constant

$$M_n = F_{n,s} - \frac{\zeta_s}{4}(F_1 + \zeta_s - 6) = \frac{2B^2}{\pi^2}\frac{\mathrm{d}^2 f_{n,s}}{\mathrm{d}s^2}(s = \pm 1)\,. \tag{A.26}$$

A more sophisticated approach is needed. Nevertheless, we encrypted at least the dependencies of the near field constant D_4.

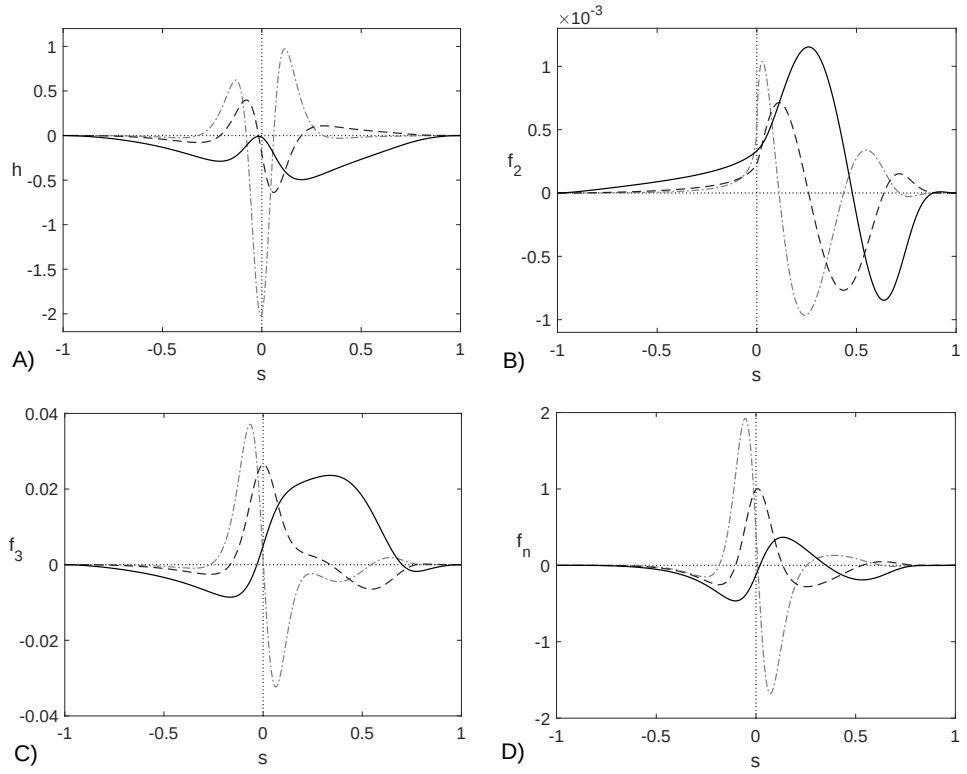

FIG. 5. *Numerical solutions of the second sublayer on the Chebyshev grid s* (4.9) *with* $N = 800$ *and* $B = 4$*, according to expansion* (4.2) *and equations* (4.3), (A.6)*. Besides the solution function (solid line), the first (dashed line) and second derivative (dash-dotted line) are visualised. A) Leading order h, after separation* (4.7)*. B) Second order* f_2*, after separation* (A.9)*. C) Third order special solution, after* (A.15)*. D) Fourth order special solution with imprecise far field, after* (A.24)*.*

A.3. Singularity structure and motion. Near the singularity ζ_s the second sublayer has the following form,

(A.27)
$$g(\zeta,\tau) \sim \tau\left[\frac{6}{(\zeta-\zeta_s)^2} - \frac{6/5}{\zeta-\zeta_s} + \dots\right] + \beta^2 D_2\left[\frac{1}{(\zeta-\zeta_s)^3} - \frac{1/10}{(\zeta-\zeta_s)^2} + \dots\right] + \\ +\beta\left[\frac{D_3}{(\zeta-\zeta_s)^3} - \frac{D_3/10}{(\zeta-\zeta_s)^2} + \frac{3/20}{(\zeta-\zeta_s)} + \dots\right] + \dots\,, \qquad \tau\to\infty\,.$$

Actually, this behaviour reminds us on the structure of a singular traveling wave (STW) solution (5.2) of the Fisher equation. To compare this two expansions, we rewrite z in dependence of ζ with the help of the inner variables (2.6) and (3.9), yielding

(A.28)
$$z(\zeta,t) = z_s \pm \sqrt{8\tau(t-t_s)}\left[1 - \frac{1}{8}\frac{\ln(\tau)}{\tau} + \frac{\zeta}{4}\frac{1}{\tau}\right].$$

We consider the singular trajectory expansion (5.3) for granted, such that

$$z(\zeta,t)-z_p(t)=\pm\sqrt{8\tau(t-t_s)}\left[\frac{\zeta-\zeta_s}{4}\frac{1}{\tau}-\eta_s\frac{\ln^2(\tau)}{\tau^2}-\delta_s\frac{\ln(\tau)}{\tau^2}-\frac{\mu_s}{\tau^2}-\dots\right]. \tag{A.29}$$

In correspondence, we perform the change of variables in the singular traveling wave (5.2) and obtain the expansion of the second sublayer (near ζ_s),

$$u(z(\zeta,t)\to z_p(t))=\frac{2}{t-t_s}g(\zeta\to\zeta_s,\tau)\,,\qquad \tau\to\infty\,, \tag{A.30}$$

if and only if $D_2=48\eta_s$, $D_3=48\delta_s$, $D_4=48\mu_s$. In other words, we managed to match (A.27) directly to a STW–solution. The same holds for the subsequent layers, beginning with the third. Since we already know the generic structure of the singular trajectory expansion (5.3), there is no need to study each subsequent layer in detail, the main dynamics do not change.

Hence, we believe the 'interaction' between the two moving singularities shortly beyond blow-up is inherited in the first two sublayers. Afterwards, the local singularity profile simplifies to a combined pole of second and first order, in form of a singular traveling wave solution. Likewise, all coefficients in the singular trajectory expansion (5.3) after ζ_s can be read out directly from the near field of the second sublayer.

We combine the determined matching relations (A.7) and the numerically found transition relations of the second sublayer (A.13, A.19, A.26), in order to obtain the corrections to the singularity motion (5.3) up to $O(\tau^{-2})$,

$$\begin{aligned}&\eta_s\approx\frac{1}{8}\left(\frac{C_2}{2}-\frac{1}{16}\right),\qquad \delta_s\approx\frac{1}{8}\left(\frac{C_3}{2}+\frac{C_1}{16}-\frac{9}{8}+\frac{M}{4}-\ln(2)\right),\\ &\mu_s=\frac{C_3}{16}+\frac{M_n}{4}-\frac{29}{32}-\frac{1}{2}\left(\frac{C_1-2}{16}-\ln(2)\right)\left(\frac{C_1-2}{16}-\ln(2)+\frac{M+1}{2}\right).\end{aligned} \tag{A.31}$$

Here, C_i are the local degrees of freedom of the initial expansion (2.4, A.1), $M\approx -0.0566$ is the invariant (constant) of g_1 (4.11) and M_n is the missing invariant of g_4, or rather g_n, (A.26). To emphasize that only two of the three singularity positions above are independent, in correspondence to (A.7), we may write

$$\mu_s=\delta_s+\frac{M_n}{4}-\frac{13}{16}+\frac{(M+1)^2-\zeta_s(\zeta_s+3)}{32}\,. \tag{A.32}$$

In combination with the result for ζ_s (4.14), we managed to encrypt the relations between the initial constants C_i and the coefficients in the singular trajectory expansion (5.3) up to $O(\tau^{-2})$. Theoretically, our approach enables us to find the relations up to any order we want, which requires solely the tracking of upcoming higher order constants, from the initial expansion through the first two asymptotic sublayers.

Appendix B. Physical background: incipient laminar-turbulent bypass transition in wall bounded flows. Viewed historically, the present study arose as a result of our efforts to investigate laminar boundary layer flows, in particular their tendency to flow separation, instability and laminar-turbulent transition, using perturbation techniques. Despite the ongoing rise in computation power and the corresponding boost in computational fluid dynamics as well as continuously improved experimental techniques, the natural or forced transition process from a laminar to a turbulent boundary layer flow is still not fully understood. Our approach to the

investigation of the early stages of this transition process is based on the framework of interaction boundary layer theory, i.e. high Reynolds number ($Re \to \infty$) asymptotics. Thereby the concerned spatial domain and the temporal evolution of the flow under investigation is split in several distinct regimes with characteristic, Re-dependent spatio-temporal scales. The associated, correspondingly simplified set of model equations result from the underlying Navier–Stokes equations in a systematic way.

To be more specific, we focus on a near-critical, so-called marginally separated flow of a nominally planar, incompressible, steady laminar boundary layer which is of particular significance, for example, in the leading edge area on the suction side of an airfoil, [22, chapter 4]. Weak three-dimensional disturbances that change over time are imposed on the basic flow such that the laminar-turbulent transition process is triggered; for details see the related studies [3, 4, 2, 5]. As these investigations show, the (local) boundary layer characteristics, namely the streamwise component of the wall shear stress (or equivalently the spanwise vorticity component at the solid wall $y = 0$) and the (negative) correction of the displacement thickness can be expressed in terms of a single quantity, say A, which under near-critical conditions expands as

$$A \sim A_c(x) + \varepsilon^2 b(x)[2u(z,t) - 1] + O(\varepsilon^4 \ln \varepsilon)\,, \qquad \varepsilon = |\Gamma_c - \Gamma|^{1/4} \to 0^+\,. \tag{B.1}$$

Here x, y, and z, t, and $\varepsilon \sim O(Re^{-1/40})$ denote the streamwise, wall-normal, and spanwise coordinates, the time, and a small perturbation (bifurcation) parameter, [20]. All involved quantities are non-dimensionalized and suitably scaled. Moreover, Γ represents a parameter controlling the magnitude of the (adverse) pressure gradient imposed on the boundary layer flow (the angle of attack in the above mentioned example), and Γ_c its critical value, up to which steady (planar) solutions of the equation for A exist. Comprehensive investigations reveal a saddle-node bifurcation at $\Gamma = \Gamma_c$ where $A = A_c(x)$, and the associated dimension reduction in its neighborhood. There the spatial structure with respect to the streamwise coordinate x is determined by the active eigenmode $b(x)$ (with zero eigenvalue) and the evolution of the system is determined by a bifurcation equation for the shape function $u(z,t)$ dependent on the other, 'inactive' variables. This amplitude equation, which actually represents a solvability condition, can be identified as a forced version of the well-known Fisher–KPP equation [10, 18, 17],

$$\frac{\partial u}{\partial t} - \frac{\partial^2 u}{\partial z^2} = u - u^2 - \frac{\theta(\Gamma - \Gamma_c)}{2} + g\,. \tag{B.2}$$

Here the forcing term $g(z,t)$ originates from the unsteady, three-dimensional perturbations imposed on the flow, and the Heaviside function $\theta(\cdot)$ is used to distinguish between the distinct cases of sub-critical, $\Gamma < \Gamma_c$, and super-critical, $\Gamma > \Gamma_c$, flows. Whereas a certain magnitude of g is required to provoke a finite-time blow-up event of (B.2) in the case of sub-critical flows when starting from the stable (planar) branch $u(z,0) = u_s = 1$, super-critical conditions lead to (repeated, self-sustained) blow-up(s) even in the absence of any forcing. Furthermore, it is found that the internal structure of a (point) blow-up singularity of (B.2) is independent of how it is caused, i.e. the specific form of g and the presence of sub- or super-critical conditions, [3].

As already mentioned in §1, here we do not face the constraint of limited ranges of u, which enables us to explore the rich and interesting dynamics of (B.2) with respect to the formation of finite-time singularities, [13], and the continuation of the solution beyond blow-up. Although the growth of u beyond all limits causes a (local) breakdown of the underlying expansions, such as (B.1), singularities are of

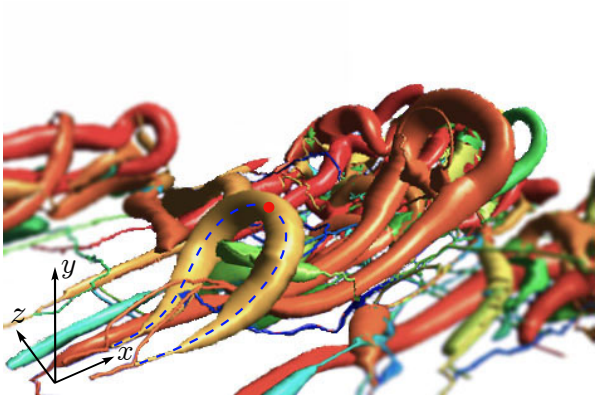

FIG. 6. *Direct numerical simulation (DNS) of a transitional boundary layer flow close to a solid wall $y = 0$: formation of hairpin vortices (ochre- and orange-colored structures), associated with the appearance of moving singularities beyond point blow-up(s) in the asymptotic description by (B.2), cf. figure 1 (main flow in x-direction). Source U. Rist, Institute of Aerodynamics and Gas Dynamics, University of Stuttgart, see also [21].*

particular interest and physical significance, because their appearance is the only way that scale changes in the asymptotic description are possible, thereby reflecting the characteristic features of vortex formation and disintegration in the incipient laminar-turbulent transition process, figure 6.

The creation of hairpin or lambda vortices is associated with the appearance of the moving singularity pair immediately beyond a point blow-up event of the Fisher–KPP equation (B.2). Compare to figure 1, where the trajectories of this singularity pair represent the temporal evolution of the vortex kernels near the surface. These singularities are commonly regularized by analyzing their internal structure, the corresponding re-scaling of the dependent and independent variables, and the ensuing derivation of adapted model equations based on the original (Navier–Stokes) equations. Nevertheless, the position of these vortical structures is fixed to the location of the moving singularities.

Acknowledgments. The authors would like to thank the reviewers for their helpful comments and suggestions.

REFERENCES

[1] J. P. BOYD, *Chebyshev and Fourier Spectral Methods*, Dover Publications, Inc., Mineola, New York, 2nd ed., 2001.

[2] S. BRAUN, *Recent developments in the asymptotic theory of separated flows. Leverhulme lectures - lecture notes*, 2006, http://eprints.maths.manchester.ac.uk/id/eprint/656. Manchester Mathematical Sciences (MiMS) EPrints.

[3] S. BRAUN AND A. KLUWICK, *Unsteady three-dimensional marginal separation caused by surface-mounted obstacles and/or local suction*, Journal of Fluid Mechanics, 514 (2004), pp. 121–152, https://doi.org/10.1017/S0022112004000187.

[4] S. BRAUN AND A. KLUWICK, *Blow-up and control of marginally separated boundary layers*, Philosophical Transactions of the Royal Society A, 363 (2005), p. 1057–1067, https://doi.org/10.1098/rsta.2005.1549. Theme Issue 'New developments and applications in rapid fluid flows', J. S. B. Gajjar and F. T. Smith, eds.

[5] S. BRAUN, S. SCHEICHL, AND D. KUZDAS, *The triple-deck stage of marginal separation*, Journal of Engineering Mathematics, 128 (2021), https://doi.org/10.1007/s10665-021-10125-3.

[6] CHEBFUN TEAM, *Chebfun – numerical computing with functions*, 2022. University of Oxford,

http://www.chebfun.org/, Retrieved November, 2022.

[7] *NIST Digital Library of Mathematical Functions*. http://dlmf.nist.gov/, Release 1.1.7 of 2022-10-15, http://dlmf.nist.gov/. F. W. J. Olver, A. B. Olde Daalhuis, D. W. Lozier, B. I. Schneider, R. F. Boisvert, C. W. Clark, B. R. Miller, B. V. Saunders, H. S. Cohl, and M. A. McClain, eds.

[8] J. W. Dold, *On asymptotic forms of reactive-diffusive runaway*, Proceedings: Mathematical and Physical Sciences, 433 (1991), pp. 521–545, http://www.jstor.org/stable/51917.

[9] M. Fasondini, J. King, and J. Weideman, *Blow up in a periodic semilinear heat equation*, Physica D: Nonlinear Phenomena, 446 (2023), p. 133660, https://doi.org/10.1016/j.physd.2023.133660.

[10] R. A. Fisher, *The wave of advance of advantageous genes*, Annals of Eugenics, 7 (1937), pp. 355–369, https://doi.org/10.1111/j.1469-1809.1937.tb02153.x.

[11] H. Fujita, *On the blowing up of solutions of the cauchy problem for* $u_t = \Delta u + u^{1+\alpha}$, Journal of the Faculty of Science. University of Tokyo. Section IA. Mathematics, 13 (1966), pp. 109–124.

[12] V. A. Galaktionov and J. L. Vazquez, *Necessary and sufficient conditions for complete blow-up and extinction for one-dimensional quasilinear heat equations*, Archive for Rational Mechanics and Analysis, 129 (1995), pp. 225–244, https://doi.org/10.1007/BF00383674.

[13] V. A. Galaktionov and J. L. Vázquez, *The problem of blow-up in nonlinear parabolic equations*, Discrete and Continuous Dynamical Systems, 8 (2002), pp. 399–433, https://doi.org/10.3934/dcds.2002.8.399.

[14] B. Hernández-Bermejo and A. Sánchez-Valdés, *Transition between extinction and blow-up in a generalized Fisher–KPP model*, Physics Letters A, 378 (2014), pp. 1711–1716, https://doi.org/10.1016/j.physleta.2014.04.027.

[15] M. Herrero and J. J. L. Velázquez, *Blow-up behaviour of one-dimensional semilinear parabolic equations*, Annales de l'Institut Henri Poincaré C, Analyse non linéaire, 10 (1993), pp. 131–189, https://doi.org/10.1016/S0294-1449(16)30217-7.

[16] L. M. Hocking, K. Stewartson, J. T. Stuart, and S. N. Brown, *A nonlinear instability burst in plane parallel flow*, Journal of Fluid Mechanics, 51 (1972), pp. 705–735, https://doi.org/10.1017/S0022112072001326.

[17] A. Kluwick, S. Braun, and E. A. Cox, *Near critical phenomena in laminar boundary layers*, Journal of Fluids and Structures, 24 (2008), pp. 1185–1193, https://doi.org/10.1016/j.jfluidstructs.2008.06.014.

[18] A. N. Kolmogorov, I. G. Petrovskii, and N. S. Piskunov, *A study of the diffusion equation with increase in the amount of substance, and its application to a biological problem*, Bull. Moscow Univ. Math. Mech., 1 (1937), p. 1–26. Reprinted in: V. M. Tikhomirov (ed.) Selected Works of A. N. Kolmogorov, vol. 1, pp. 242–270. Kluwer, Dordrecht (1991). Also in: I. G. Petrowsky Selected Works, Part II, pp. 106–132. Gordon and Breach, Amsterdam (1996).

[19] S. W. McCue, M. El-Hachem, and M. J. Simpson, *Exact sharp-fronted travelling wave solutions of the Fisher–KPP equation*, Applied Mathematics Letters, 114 (2021), p. 106918, https://doi.org/10.1016/j.aml.2020.106918.

[20] S. Scheichl and A. Kluwick, *On the effects of compressibility in marginally separated flows*, Proceedings in Applied Mathematics and Mechanics, 8 (2008), pp. 10639–10640, https://doi.org/10.1002/pamm.200810639.

[21] S. Stegmaier, U. Rist, and T. Ertl, *Opening the can of worms: an exploration tool for vortical flows*, in VIS 05. IEEE Visualization, 2005, pp. 463–470, https://doi.org/10.1109/VISUAL.2005.1532830.

[22] V. V. Sychev, A. I. Ruban, V. V. Sychev, and G. L. Korolev, *Asymptotic Theory of Separated Flows*, Cambridge University Press, Cambridge, 1998.

[23] L. N. Trefethen, *Spectral Methods in MATLAB*, SIAM, Philadelphia, 2000.

[24] M. Van Dyke, *Perturbation methods in fluid mechanics*, The Parabolic Press, Stanford, California, 1975.

[25] J. A. C. Weideman, *Computing the dynamics of complex singularities of nonlinear PDEs*, SIAM Journal on Applied Dynamical Systems, 2 (2003), pp. 171–186, https://doi.org/10.1137/S1111111102398305.